Reaction Kinetics, Mechanisms and Catalysis (2022) 135:3375–3391
https://doi.org/10.1007/s11144-022-02281-z

Magnetic properties and photocatalytic activity of $Bi_{1-x}Sm_xFe_{1-y}Ni_yO_3$ nanoparticles for methyl red degradation

Ava Saghafi[1] · Razieh Sanavi Khoshnood[1] · Davoud Sanavi Khoshnoud[1,2] · Zarrin Es'Haghi[1,3]

Received: 19 June 2022 / Accepted: 9 August 2022 / Published online: 1 October 2022

Abstract

In this work, $Bi_{1-x}Sm_xFeO_3$ (x = 0.1, 0.08, 0.06, 0.04, 0.02) and $Bi_{0.094}$ $Sm_{0.06}$ Fe_{1-y} Ni_yO_3 nanoparticles (y = 0.05, 0.03, 0.01) were synthesized by sol–gel method. The structural, microstructural, magnetic, and optical properties of $Bi_{1-x}Sm_xFe_{1-y}Ni_yO_3$ nanoparticles were characterized by using X-ray diffraction, field-emission scanning electron microscopy, the energy-dispersive X-ray analysis, vibrating sample magnetometry and UV–Vis reflectance spectra at room temperature. The structural investigations indicate that the unit cell volume decreases with Sm ion doping, while it increases with substituting Ni ions in the $Bi_{1-x}Sm_xFe_{1-y}Ni_yO_3$ nanoparticles. Moreover, the magnetic properties were enhanced by doping Sm and Ni ions. The photocatalytic activities of $Bi_{1-x}Sm_xFe_{1-y}Ni_yO_3$ nanoparticles were investigated to degrade methyl red (M.R.) in an aqueous solution. For this purpose, the M.R. degradation with the synthesized photocatalysis was evaluated at room temperature under dark and visible light exposure using a mercury lamp (150 W). The results indicated that the highest photodegradation of M.R. is obtained using $Bi_{0.94}Sm_{0.06}Ni_{0.03}Fe_{0.97}$ nanoparticles as a photocatalyst in the presence of hydrogen peroxide in an acidic media (pH 3). Besides, the photocatalytic activity of $Bi_{1-x}Sm_xFe_{1-y}Ni_yO_3$ (x = 0.06, and y = 0.01, 0.03, 0.05) is higher than that of $Bi_{1-x}Sm_xFeO_3$ (x = 0.0, 0.02, 0.04, 0.06, 0.08) nanoparticles for the photodegradation of MR. Besides, the Sm and Ni co-doped BFO nanoparticles have a greater magnetic property than the Sm-doped BFO nanoparticles, leading to a simple and fast separation of catalyst using a strong magnet after the M.R. degradation. Under the optimum conditions, the M.R. degradation efficiencies under visible-light illumination for 60 and 100 min were 97.34 and 85.76% for $Bi_{0.94}Sm_{0.06}Ni_{0.03}Fe_{0.97}$ and $Bi_{094}Sm_{0.06}FeO_3$ nanoparticles at pH 3.0.

Keywords Nanoparticles · Bismuth Ferrite · Sol–gel · Photocatalyst · Methyl red degradation

---

✉ Razieh Sanavi Khoshnood
rskhoshnood@yahoo.com

Extended author information available on the last page of the article

Introduction

Today, a wide variety of industrial products are produced with the expansion of various industries to create human comfort. Many of these products are led to environmental pollution by an uncontrolled discharge of non-usable textiles, reactants, and reagents into the environment [1, 2]. This problem becomes acute when these pollutants are non-biodegradable and accumulate in the environment [3, 4]. These pollutants eventually enter the human and animal bodies through food chains and cause many human and animal health [5–7].

Photocatalytic processes are widely applied to degrade non-biodegradable pollutants[8, 9]. The advantages of the procedure include simplicity and low-cost operation, no production of secondary pollutants, and performing the process at ambient pressure and temperature[10]. It can also be utilized for large-scale practical applications [11]. Various methods were applied to enhance the photocatalytic efficiency of a photocatalyst toward pollutant degradation, including selecting a suitable photocatalyst, doping with various materials, preparing composites by mixing suitable semiconductors with proper morphology and crystallography phase, and modifing the photocatalyst surface with appropriate functional groups [12]. Among them, doping with a suitable nanoparticle, metal ion, nanocomposite, etc., significantly impacts the efficiency of the photocatalytic process, which is a critical method to improve the photocatalytic properties of semiconductors [13–17].

Bismuth ferrite (BFO) is a multiferroic compound with simultaneous ferromagnetic and ferroelectric properties used to manufacture spintronics, sensors, piezoelectric devices, memory, and photovoltaics [11, 18]. BFO has shown suitable photocatalytic properties under visible light for the degradation of organic material because of the narrow and low band-gap energy of 2.2 eV [18–22]. Besides, BFO as a photocatalyst can be quickly and easily separated from the sample solution in the presence of a strong magnet[23]. Other advantages of BFO as a photocatalyst are simple synthesis and modification, cheapness, and chemical and thermal stability. However, the photocatalytic activity of BFO is limited due to the high rate of electrons and holes combination, the narrow range of the photoresponse, and the low conduction band level[24–26]. A straightforward and effective way to overcome this limitation is to dope the appropriate metals into the BFO network, enhancing the absorptivity of visible light and the separation properties of charge carriers with an increase in surface area photocatalyst through heterojunction formation [11]. Recently, there has been a strong tendency to simultaneously dope two metals into the BFO structure, which leads to a further modification in the photocatalyst activity than BFO doping with a metal [10]. For example, using two metals (Ni and Nd) doped in BFO increased the transfer rate of the generated electron in the BFO network. It significantly prevented the recombination of the electron and the hole produced in the BFO structure [27, 28]. Similarly, an increase in photocatalytic activity with co-doped (La^{3+} and Se^{4+}) in BFO is due to increased absorption efficiency of light, proper separation of photogenerated charge carriers, and a decrease in the recombination rate of the hole–electron pairs [29]. However, the type and percentage of dopants selected in the preparation of photocatalyst based on co-doped BFO are very effective in its activity.

In the study, two BFO derivatives including In this work, $Bi_{1-x}Sm_xFeO_3$ ($x = 0.1$, 0.08, 0.06, 0.04, 0.02) and $Bi_{0.094}$ $Sm_{0.06}$ Fe_{1-y} Ni_yO_3 nanoparticles ($y = 0.05$,0.03,0.01) were synthesized by sol–gel method. The ability of these nanoparticles as photocatalysts in the methyl red degradation process was investigated and compared. Various methods characterize the structural, morphology, and magnetic properties of these nanoparticles. The photocatalytic activities of Sm-doped BFO and Sm and Ni co-doped BFO for the degradation of methyl red in an aqueous solution were evaluated under dark and visible light conditions at room temperature. The advantages of the synthesis photocatalysis (Sm and Ni co-doped BFO nanoparticles and Sm-doped BFO nanoparticles) for the M.R. degradation include straightforward preparation, low cost, high degradation efficiency, and suitable degradation time under visible light.

Experimental

Reagents and materials

All materials used to synthesize the photocatalyst, including bismuth (III) nitrate pentahydrate, iron (III) nitrate nonahydrate, samarium (III) nitrate hexahydrate, and nickel (II) nitrate hexahydrate, nitric acid, tartaric acid, ammonium hydroxide (28%), were purchased from Merck (Germany). Methyl red (M.R.) with an analytical grade was obtained from Sigma Aldrich (USA).

Instruments

A UV–visible spectrophotometer (Varian Cary Bio 50 model) was used to determine the M.R. concentration in the aqueous solution. The morphology and structure of $BiFeO_3$ (BFO), $Bi_{1-x}Sm_x$ $FeO_{3,}$ and $Bi_{1-x}Sm_x$ $Fe_{1-y}Ni_yO_3$ as a photocatalyst were investigated using X-ray diffraction spectroscopy (XRD; Bruker D8 ADVANCE, Germany), the field-emission scanning electron microscopy (FE-SEM; Mira 3 Tescan; Czech Republic), and vibration sample magnetometry (VSM; analysis under applied magnetic fields up to 20 kOe at 300 K). A mercury lamp (150 W) was utilized to study the photocatalytic activity of $BiFeO_3$ (BFO), $Bi_{1-x}Sm_x$ $FeO_{3,}$ and $B_{(1-x}Sm_x$ $Fe_{1-y}Ni_yO_3$ for the M.R. degradation under visible light at a distance of about 5 cm from the M.R. aqueous solution. A Metrohm pH meter (model 780, Switzerland) was applied to adjust the pH of the M.R. aqueous solution.

Photocatalyst preparation

The nanoparticles of $BiFeO_3$ (BFO), $Bi_{(1-x)}Sm_xFeO_3$ ($x = 0.1$, 0.08, 0.06, 0.04, 0.02) and $Bi_{0.094}$ $Sm_{0.06}$ Fe_{1-y} Ni_yO_3 nanoparticles ($y = 0.05$,0.03,0.01) as a photocatalyst were prepared according to the sol–gel technique. The photocatalyst was synthesized using a reported paper with a little modification [45]. For this purpose, an appropriate amount of bismuth nitrate, iron(III) nitrate, samarium(III) nitrate, and nickel(II) nitrate was poured into a solution containing 1.0 mL of nitric acid and 20.0 mL of distilled water. The mixture was stirred at 500 rpm for 1 h at 60 °C to dissolve all compounds, followed by tartaric acid completely. The mixture was stirred at room temperature for 2 h, and a milky color suspension was formed. While the suspension was continuously stirred, an aqueous ammonia solution (20% or 2 mol L^{-1}) was added dropwise to the suspension until its pH reached about 3. The suspension was stirred for 9 h with an initial temperature of 80 °C, which increased to 200 °C at a rate of 1 °C min^{-1} and remained constant at the temperature. The mixture was finally calcined in a digital furnace at temperatures of 400 °C for 6 h and 600 °C for 5 h.

Photodegradation procedure

A homemade photocatalytic reactor was fabricated with dimensions of $75\times50\times40$ Cm^3, including two fans to control its temperature, a Hg vapor lamp, and a magnetic stirrer to perform the M.R. degradation under visible light irradiation. For this purpose, 185.0 mL of M.R. aqueous solution (2.9 mg L^{-1}) was poured into a proper beaker, and its pH was adjusted to 3.1 using hydrochloric acid solution (0.1 mol L^{-1}). Then, catalyst (98 mg), and H_2O_2 solution (0.58 mL), were added to the resulting solution. The resulting suspension was diluted to 200.0 ml with distilled water. The suspension was transferred into the photocatalytic reactor. The suspension was stirred at 600 rpm for 5.0 h at room temperature in the dark to achieve an adsorption–desorption equilibrium. The suspension was exposed for a suitable time, and sampling was carried out using a pipette every 10 min, followed by centrifuging for 10 min at 5000 pm. The mixture was filtered, and the solution was determined by the spectrophotometric method at 521.9 nm. The degradation efficiency of M.R. (E%) was calculated by the following equation[12]:

$$E = \frac{\left(C_o - C_t\right)}{C_o} \times 100 \tag{1}$$

C_t and C_o are the M.R. concentration at irradiation time ($t > 0$) and initial M.R. concentration ($t=0$).

Results and discussion

Nanoparticles characterization

The XRD patterns of $Bi_{1-x}Sm_xFe_{1-y}Ni_yO_3$ nanoparticles are presented in Fig. 1(a, b). By using X'pert software, the XRD patterns of studied samples were compared with the standard diffraction data (JCPDS file No. 01-07-2494) of the $BiFeO_3$ sample. It is observed that all samples have the rhombohedral structure with a space

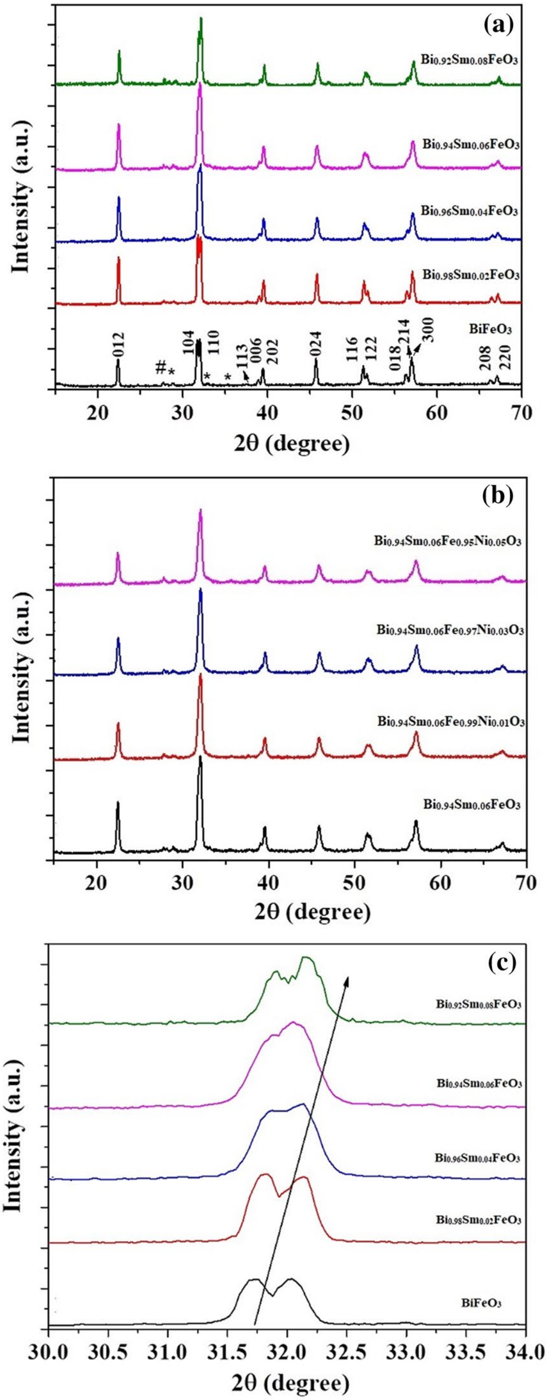

Fig. 1 X-ray diffraction patterns of **a** $Bi_{1-x}Sm_xFeO_3$ **b** $Bi_{0.94}Sm_{0.06}Fe_{1-y}Ni_yO_3$ nanoparticles **c** Magnified pattern of main peak in $Bi_{1-x}Sm_xFeO_3$ nanoparticles

group of R3c. A small amount of $Bi_2Fe_4O_9$ and Bi_2O_3 impurity phases corresponding to the JCPDS file numbers (01-072-1832) and (01-074-1374) are observed in the XRD pattern of our samples that were displayed with symbols (*) and (#). It is clear that the amount of impurity phases decreases with increasing Sm content, but these gradually increase with increasing Ni content, again. This effect was also observed in the literature [30]. On the other hand, the doublet peaks in the XRD patterns merge gradually to one peak with increasing Sm concentration. This effect indicates that distortion occurs in the rhombohedral structure because of the difference in radii ionic between Bi^{3+} and Sm^{3+} ions. However, because of the small difference between the radii ionic of Fe^{3+} and Ni^{3+} ions, Ni substitution does not modify the XRD pattern of $Bi_{0.94}Sm_{0.06}Fe_{1-y}Ni_yO_3$ nanoparticles significantly. Moreover, Fig. 1c indicates the magnified major peaks of the XRD patterns. It is clear that the peaks shifted slightly toward higher angles with increasing Sm^{3+} concentration. Thus, based on Bragg's law, the lattice parameters decrease. Hence, the lattice constants (a, b, and c) and unit cell volume (V) of $Bi_{1-x}Sm_xFe_{1-y}Ni_yO_3$ nanoparticles were calculated using the Fullprof software. Fig. S1 illustrates the Rietveld refinement of the XRD pattern for the studied samples. Their results are listed in Table 1. The results indicate that unit cell volume decrease with Sm substitution. This occurrence can be attributed to the replacement of Bi^{3+} ion with radii ionic of 1.03 Å by Sm^{3+} ion with radii ionic of 0.958 Å [31, 32]. This result agrees with the previous report [33]. In contrast, the unit cell volume increase with Ni substituting in $Bi_{0.94}Sm_{0.06}Fe_{1-y}Ni_yO_3$ nanoparticles. This irregular effect may be ascribed to substituting Fe^{3+} ion with radii ionic of 0.645 Å in the photocatalyst composite by low valance Ni ion (Ni^{2+}) with radii ionic of 0.69 Å [34].

The FE-SEM images of $Bi_{1-x}Sm_xFe_{1-y}Ni_yO_3$ nanoparticles are presented in Fig. S2. By comparing the insets of Fig. S2, the size particle distribution histograms, can be concluded that particle size decrease gradually with Sm doping. Moreover, the shape of $Bi_{1-x}Sm_xFe_1O_3$ particles does not modify with Sm substitution. On the other hand, the effect of Ni substitution in the $Bi_{0.94}Sm_{0.06}FeO_3$ sample is more effective on particle size, as shown in insets of Fig. S2. Furthermore, the porosity of samples increases with Fe^{3+} ion substitution with Ni^{2+} ion.

The energy-dispersive X-ray spectroscopy spectra of $Bi_{1-x}Sm_xFe_{1-y}Ni_yO_3$ nanoparticles are presented in Fig. S3. The patterns of $Bi_{1-x}Sm_xFe_{1-y}Ni_yO_3$

Table 1 Lattice parameters and unit cell volume of $Bi_{1-x}Sm_xFe_{1-y}Ni_yO_3$ nanoparticles

Sample	a = b (Å)	c (Å)	V (Å)^3
$BiFeO_3$	5.577(2)	13.866(1)	373.5(2)
$Bi_{0.98}Sm_{0.02}FeO_3$	5.575(4)	13.856(3)	373.0(1)
$Bi_{0.96}Sm_{0.04}FeO_3$	5.576(1)	13.844(0)	372.7(8)
$Bi_{0.94}Sm_{0.06}FeO_3$	5.574(7)	13.833(8)	372.3(2)
$Bi_{0.92}Sm_{0.08}FeO_3$	5.570(4)	13.822(4)	371.4(4)
$Bi_{0.94}Sm_{0.06}Fe_{0.99}Ni_{0.01}O_3$	5.577(4)	13.828(3)	372.5(4)
$Bi_{0.94}Sm_{0.06}Fe_{0.97}Ni_{0.03}O_3$	5.577(4)	13.833(2)	372.6(7)
$Bi_{0.94}Sm_{0.06}Fe_{0.95}Ni_{0.05}O_3$	5.579 (1)	13.833(2)	372.8(9)

nanoparticles ($y=0.0$) were composited of four elements, including Bi, Sm, Fe, and O, without the presence of any other elements in the obtained pattern. The peak intensity of Bi in BFO was reduced with doping Sm in the BFO composite, confirming that Bi ions in BFO were successfully substituted with Sm ions. Also, five elements, Bi, Fe, Sm, Ni, and O, are observed in the pattern of $Bi_{0.94}Sm_{0.06}$ $Fe_{1-y}Ni_{y}O_{3}$ nanoparticles, which indicates any other peaks of elements are not present in the obtained pattern of these nanoparticles. Similarly, a decrease in the peak intensity of Fe ions in BFO was observed by substituting them with Ni ions. The results indicated the successful synthesis of $Bi_{1-x}Sm_{x}Fe_{1-y}Ni_{y}O_{3}$ nanoparticles with a high purity without other elements in the structure of these nanoparticles.

The magnetic hysteresis loop (M–H) of $Bi_{1-x}Sm_{x}Fe_{1-y}Ni_{y}O_{3}$ nanoparticles at room temperature (R.T.) was observed in Fig. 2. It is clear that BFO indicates an antiferromagnetic behavior with not any hysteresis loop. However, with doping Sm in BFO, the $Bi_{1-x}Sm_{x}FeO_{3}$ nanoparticles exhibit a weak ferromagnetic feature. It is known that the magnetic behaviour of $BiFeO_{3}$ is due to two components. The first one consists of a short-range order due to the sublattice of Fe^{3+} ions. The second one includes a long-range order that has the spiral spin structure with a long wavelength of $\lambda=62$ nm[35]. Therefore, a suppression occurs in the spiral cycloid spin structure via modifying short-range order due to structural distortion by Sm substitution. As a result, the remnant magnetization (M_{r}) and coercive field ($H_{.C.}$) increase with Sm concentration, as shown in Table 2. On the other hand, the effect of Ni substitution on the magnetic behaviour of the $Bi_{0.94}Sm_{0.06}FeO_{3}$ sample is different compared to that of Sm substitution in BFO. While M_{r} enhances with increasing Ni doping, but $H_{.C.}$ decline with them. As mentioned in the structural part, because the Ni ionic radii is almost similar to that of Fe, the change in magnetic behavior because of lattice distortion is weakened. Therefore, two scenarios are possible for modifying the magnetic behaviour of the $Bi_{0.94}Sm_{0.06}Fe_{1-y}Ni_{y}O_{3}$ sample. (i) Difference of magnetic moment between Fe ion and Ni ion; With substituting Ni ion for Fe ion, there is a non-zero contribution in magnetization because of the imbalance of the magnetic moment of Fe (5 μ_{B}) and Ni (2 μ_{B}) in B site. However, this factor is not very dominant due to the low-level Ni ion doping. (ii) Size effect; When the average particle size is less than 62 nm, this factor plays an important role in the magnetic behavior of studied samples. The microstructural result of $Bi_{1-x}Sm_{x}Fe_{1-y}Ni_{y}O_{3}$ nanoparticles indicates that the particle size decrease more with Ni doping so that it is clear, particularly in the sample with $y=0.05$. Therefore, we expect that M_{r} increase and $H_{.C.}$ decrease with decreasing particle size. These results were supported by previous reports [36, 37].

In order to investigate the optical properties of $Bi_{1-x}Sm_{x}Fe_{1-y}Ni_{y}O_{3}$ nanoparticles at RT, the UV–Vis diffuse reflectance spectra were carried out in 100–1200 nm wavelength. Fig. S4 shows the changes of $[F(R)h\nu]^{2}$ versus $h\nu$ (photon energy) for $Bi_{1-x}Sm_{x}Fe_{1-y}Ni_{y}O_{3}$ nanoparticles. The adsorption [F(R)] spectra of all samples were calculated using Kabelka–Munk (K–M) equation [38]. The direct band gap of $Bi_{1-x}Sm_{x}Fe_{1-y}Ni_{y}O_{3}$ nanoparticles was determined using plotted curves in Fig. S4. The band gap of $Bi_{1-x}Sm_{x}FeO_{3}$ nanoparticles ($x=0.0$, 0.02, 0.04, 0.06, 0.08) were deduced about 2.14, 2.12, 2.12, 2.06, and 2.14 eV. The decrease of band gap

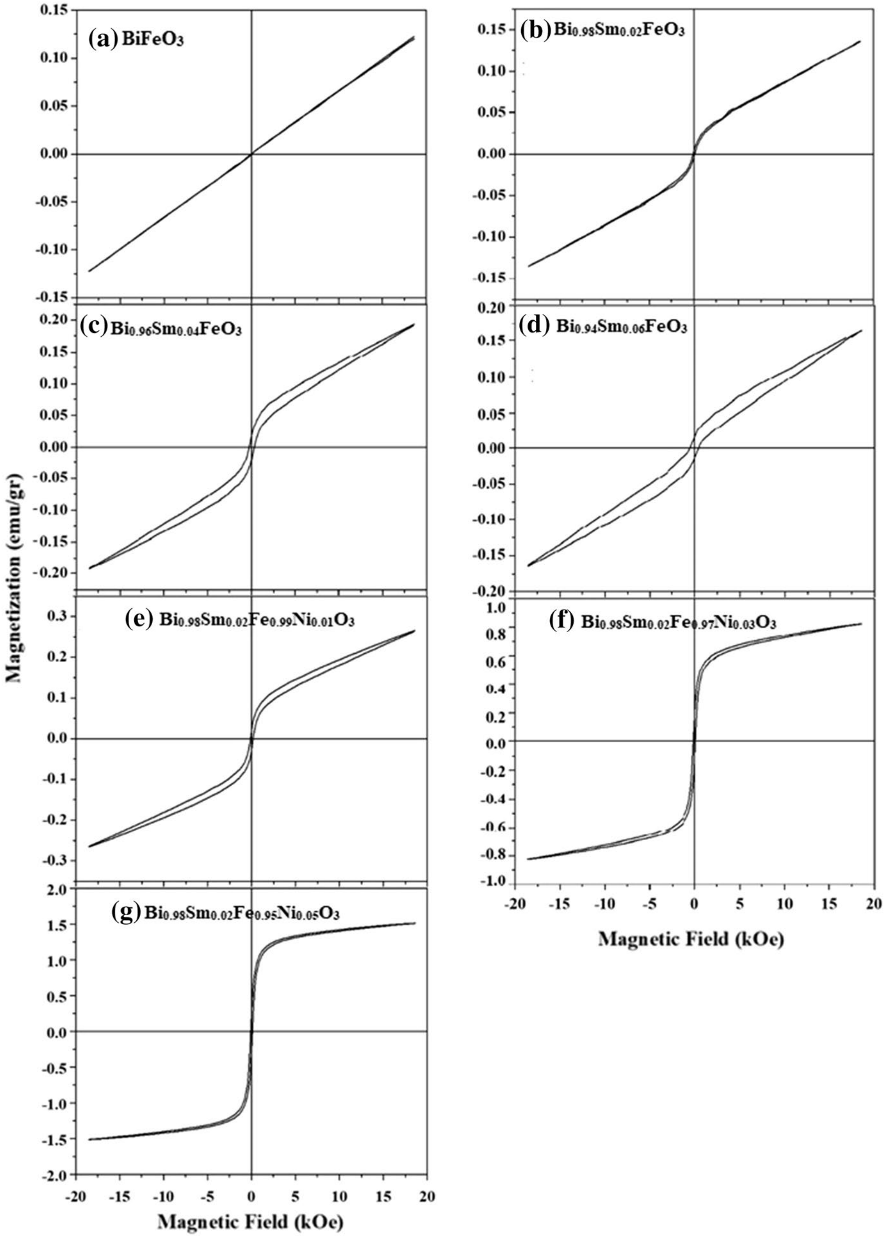

Fig. 2 Magnetic hysteresis loop of Magnetic parameters of the prepared photocatalyst ($Bi_{1-x}Sm_xFe_{1-y}Ni_yO_3$ nanoparticles) at room temperature

with Sm doping is agreed with a previous report [39]. Besides, the band gaps of $Bi_{0.94}Sm_{0.06}Fe_{1-y}Ni_yO_3$ nanoparticles decrease with Ni substituting up to $y = 0.03$ and increase afterwords (Table S1).

Table 2 Magnetic parameters of $Bi_{1-x}Sm_xFe_{1-y}Ni_yO_3$ nanoparticles at R.T

Sample	M_r(emu/gr)	H_c(Oe)	M_S(emu/gr)
$BiFeO_3$	0.00	0.0	0.120
$Bi_{0.98}Sm_{0.02}FeO_3$	0.005	100	0.140
$Bi_{0.96}Sm_{0.04}FeO_3$	0.015	286	0.180
$Bi_{0.94}Sm_{0.06}FeO_3$	0.015	519	0.170
$Bi_{0.94}Sm_{0.06}Fe_{0.99}Ni_{0.01}O_3$	0.025	150	0.260
$Bi_{0.94}Sm_{0.06}Fe_{0.97}Ni_{0.03}O_3$	0.150	110	0.820
$Bi_{0.94}Sm_{0.06}Fe_{0.95}Ni_{0.05}O_3$	0.260	92	1.510

Optimization of photodegradation procedure

A central composite design with a random order, including 30 runs, was provided to optimize four factors that affected the M.R. photodegradation. The factors run and degradation efficiencies (E%) are presented in Table 3. In the procedure, BFO was selected as a catalyst for 120 min underexposure with a U.V. lamp. Each run was repeated three times under the same condition, and the average of the results was used to calculate E% based on Eq. 1. The obtained E% was evaluated using variance analysis (ANOVA) at a confidence interval of 95% (Table 4) [40, 41]. The p-value is a suitable parameter in the ANOVA table to investigate the significance of factors or interactions[42, 43]. Therefore, all factors significantly affect the M.R. degradation due to a p-value lower than 0.05 at 95% of the confidence interval. Besides, the p-value of interaction between the M.R. concentration and catalyst amount is equal to 0.9454, indicating this interaction has a non-significant effect on the Mr degradation. Other binary interactions are meaningful parameters with a p-value lower than 0.05. The model presented using the design is significant because the p-value of the model is lower than 0.05, while the p-value of lack of fit is equal to 0.7951. Hence, the parameter is non-significant. A quadratic equation was usually developed to describe the proposed model. This equation shows the relationship between E% with factors and interactions. The resulting equation is as follows:

$$\begin{aligned} E\% = {} & 33.526 + 5.41833 * A - 7.515 * B + 5.05833 * C + 5.89833 \\ & * D - 3.2225 * AB + 0.0625 * AC + 2.4125 * AD + 3.0125 \\ & * BC - 1.9375 * BD + 5.8775 * CD - 1.22692 * A^2 + 0.0230833 \\ & * B^2 - 1.22692 * C^2 - 1.22692 * D^2 \end{aligned} \tag{2}$$

The equation's adjusted coefficient of determination (adjusted R^2) and determination coefficient (R^2) are 0.9250 and 0.9625, indicating that the equation fitted with the results well. Besides, an adequately predicted coefficient of determination (predicted R^2) of 0.8499 showed that E% could be well predicted using the equation for future investigation. The pH of samples (B) is a critical factor with a negative effect on E% due to a high and negative coefficient, indicating that the M.R. degradation is performed more effectively under acid conditions. This may be due to the better and faster decomposition of H_2O_2 in acidic media to form free radicals. The next crucial

Table 3 Central composite design for optimizing the M.R. photodegradation

Factor	Name	Unite	Low level	High level	Low amount	High amount
A	MR concentration	mg L^{-1}	− 1.0000	1.0000	1.0	3.0
B	pH	–	− 1.0000	1.0000	3.0	6.0
C	Catalyst amount	mg	− 1.0000	1.0000	50	100
D	H_2O_2 volume	mL	− 1.0000	1.0000	0.2	0.6

Std run	Run	A	B	C	D	E%
22	1	0	0	2	0	40.86
27	2	0	0	0	0	28.16
21	3	0	0	− 2	0	15.46
16	4	1	1	1	1	45.6
24	5	0	0	0	2	42.54
26	6	0	0	0	0	28.16
17	7	− 2	0	0	0	17.24
2	8	1	− 1	− 1	− 1	39.42
19	9	0	− 2	0	0	47.44
3	10	− 1	1	− 1	− 1	20.02
23	11	0	0	0	− 2	13.78
6	12	1	− 1	1	− 1	34.34
13	13	− 1	− 1	1	1	39.36
20	14	0	2	0	0	18.88
10	15	1	–	− 1	1	50.62
5	16	− 1	− 1	1	− 1	21.8
18	17	2	0	0	0	39.08
25	18	0	0	0	0	28.16
11	19	− 1	1	− 1	1	5.82
12	20	1	1	− 1	1	15.12
9	21	− 1	− 1	− 1	1	28.68
4	22	1	1	− 1	− 1	18.92
14	23	1	− 1	1	1	61.3
15	24	− 1	1	1	1	36.3
29	25	0	0	0	0	28.16
8	26	1	1	1	− 1	18.64
7	27	− 1	1	1	− 1	18.74
28	28	0	0	0	0	28.16
1	29	− 1	− 1	− 1	− 1	26.88

factor is the H_2O_2 volume (D), which has a significant coefficient in the equation and positively affects the M.R. degradation. Also, the interaction between catalyst amount and H_2O_2 volume (CD) has the highest significant and positive effect on E%. The surface plot of this interaction (CD) is presented in Fig. S5, showing that E% was increased with a simultaneous increase in catalyst amount and H_2O_2 volume. The adsorption of light was increased with increasing the catalyst amount, leading

Table 4 Analysis of variance for optimizing the M.R. photodegradation

Source	Sum of Squares	df	Mean Square	F-value	p-value	Significant
Model	4619.24	14	329.95	25.66	<0.0001	+
A-MR concentration	704.60	1	704.60	54.80	<0.0001	+
B-pH	1355.41	1	1355.41	105.42	<0.0001	+
C-catalyst amount	614.08	1	614.08	47.76	<0.0001	+
D-H_2O_2 volume	834.97	1	834.97	64.94	<0.0001	+
AB	166.15	1	166.15	12.92	0.0029	+
AC	0.0625	1	0.0625	0.0049	0.9454	–
AD	93.12	1	93.12	7.24	0.0176	+
BC	145.20	1	145.20	11.29	0.0047	+
BD	60.06	1	60.06	4.67	0.0485	+
CD	552.72	1	552.72	42.99	<0.0001	+
A^2	39.06	1	39.06	3.04	0.1033	–
B^2	0.0138	1	0.0138	0.0011	0.9743	–
C^2	39.06	1	39.06	3.04	0.1033	–
D^2	39.06	1	39.06	3.04	0.1033	–
Residual	180.00	14	12.86			
Lack of fit	104.58	10	10.46	0.5547	0.7951	–
Pure error	75.42	4	18.85			
Cor total	4799.24	28				

to an increase in the formation of electron–hole pairs and free radicals. Also, the M.R. photodegradation was significantly increased by an increase in H_2O_2 volume due to an increase in the formation of *O.H. radicals in the surface of BFO or doped BFO based on the following equation [44, 45]:

$$BFO + h\nu \rightarrow h^+ + e^- \tag{3}$$

$$H_2O_2 + e^-_{CB} \rightarrow OH^- +^* OH \tag{4}$$

$$H_2O_2 + O_2^- \rightarrow OH^- +^* OH + O_2 \tag{5}$$

This process reduces the recombination time of the electron–hole pairs and increases the M.R. degradation efficiency. The optimization of all factors was investigated based on the proposed model and equation. For this purpose, a maximum amount of E% was selected to determine the optimum amount of factors. The optimum value of M.R. concentration, pH, catalyst amount, and H_2O_2 volume was 2.9 mg L^{-1}, 3.1, 98 mg, and 0.58 mol L^{-1} (Fig. S6).

Photocatalytic activity study

Methyl red (M.R.) was selected as a typical dye to investigate the photocatalytic activity of the $Bi_{0.94}Sm_{0.06}$ $Fe_{0.97}Ni_{0.03}O_3$ nanoparticles than the $Bi_{0.94}Sm_{0.06}FeO_3$ nanoparticles in an aqueous solution of M.R. under visible-light irradiation at room temperature. In the study, the M.R. concentration and the photocatalyst amount were 2.9 mg $L^{-1}$and 98 mg at a pH of 3.1y (Sect. 2.4). The suspension of M.R. and photocatalyst (200.0 mL) was kept in the dark and stirred at 600 rpm for 5.0 h at room temperature to achieve an adsorption–desorption equilibrium. The suspension was exposed to visible light with a wavelength range between 350 and 700 nm at intervals of 0–100 min for the $Bi_{0.94}Sm_{0.06}FeO_3$ nanoparticles and 0–60 min for the $Bi_{0.94}Sm_{0.06}$ $Fe_{0.97}Ni_{0.03}O_3$ nanoparticles under magnetic stirring at room temperature. A distance of about 5 cm between the M.R. solution and the lamp was used for the light exposure. Then, the photocatalyst was separated from the suspension using a neodymium magnet. The degradation of M.R. was investigated by measuring the absorbance of the M.R. aqueous solution after separating the photocatalyst using a UV–visible spectrophotometer at a wavelength of 526.0 nm (Fig. S7). For this purpose, the absorption peak intensity of M.R. was compared with its initial intensity ($C_t/C_{.O.}$).

The photocatalytic activity of the Bi_{1-x} Sm_x FeO_3 and the $Bi_{0.094}$ $Sm_{0.06}$ Fe_{1-y} Ni_yO_3 nanoparticles is presented in Fig. S8. According to Fig. S8, the degradation efficiency of M.R. is negligible without increasing the photocatalyst, indicating that H_2O_2 has a non-significant effect on the degradation of M.R. In contrast, it increases dramatically in the presence of BFO as a photocatalyst. Besides, the photocatalytic activity of the Bi_{1-x} Sm_x FeO_3 nanoparticles increased by increasing the amount of Sm in the BFO nanoparticles. The MR degradations of 47.89, 63.21, 69.84, 85.76, and 78.51 were obtained for $x=0.00$, 0.02, 0.04, 0.06 and 0.08 in the Bi_{1-x} Sm_x FeO_3 nanoparticles for 100 min. Therefore, the highest degradation of M.R. was determined using the $Bi_{0.094}Sm_{0.06}FeO_3$ nanoparticles as a photocatalyst. Then, the effects of changing the Ni amount on the structure of the $Bi_{0.094}$ $Sm_{0.06}$ Fe_{1-y} Ni_yO_3 nanoparticles were evaluated as photocatalysts for the M.R. degradation (Fig. S8b). The results indicated that the M.R. degradations of 61.64, 80.24, 97.34, and 84.44% were obtained for $y=0.00$, 0.01, 0.03, 0.05 in the $Bi_{0.094}$ $Sm_{0.06}$ Fe_{1-y} Ni_yO_3 nanoparticles for 60 min. According to Fig. S8 b, the M.R. degradation was increased with increasing Ni^{2+} ion up to 0.03% and decreasing afterward. Because Sm^{3+} and Ni^{2+} ions can act as good electron acceptor species in the BFO structure, forming trapping sites, possibly leading to easy separation of the formed electron–hole pairs and prolonging the charge carrier lifetime[46, 47]. Excessive amounts of Sm^{3+} and Ni^{2+} dopants can form the recombination centers in the BFO lattice; as a result, the photoactivity of the prepared nanoparticles is reduced [47]. Therefore, the highest M.R. degradation of 97.34% was observed for the $Bi_{0.94}$ $Sm_{0.06}$ $Fe_{0.097}$ $Ni_{0.03}O_3$ nanoparticles as a photocatalyst at a time of about 60 min. The energy gaps of BFO, Bi_{1-x} Sm_x FeO_3, and $Bi_{0.96}Sm_{0.06}$ $Fe_{1-y}Ni_yO_3$ were studied to investigate the photocatalytic activity of these nanoparticles (Table S1 and Fig. S4). The energy gap for BFO was 2.14 eV, which decreased with increasing Sm (III) ions up to 0.06 as a dopant to 2.06 eV and increased afterward. Therefore, the highest photocatalytic activity was obtained for $Bi_{0.94}$ $Sm_{0.06}$ FeO_3 with the lowest energy band gap. Besides, investigation of energy gaps of $Bi_{0.96}Sm_{0.06}$ $Fe_{(1-y)}Ni_yO_3$ indicated that a reduction in the energy gaps was displayed with increasing Ni(II) ions as co-dopant in up to 0.03 $Bi_{0.94}$ $Sm_{0.06}$ FeO_3. Then, the energy gaps were increased for higher amounts of Ni (II) ions (Fig. S4). These results confirm that BFO photocatalytic activity to degrade M.R. increases dramatically with increasing Sm^{3+} and Ni^{2+} ions in its structure and decreases the M.R. degradation time.

The kinetics of the M.R. photodegradation in the presence of the Bi_{1-x} Sm_x FeO_3 and $Bi_{0.094}$ $Sm_{0.06}$ Fe_{1-y} Ni_yO_3 nanoparticles were investigated using the Langmuir–Hinshelwood model through the determination of the pseudo-first-order rate constant for the M.R. photodegradation. For this purpose, the pseudo-first-order rate constant for the M.R. photodegradation was determined based on the following nonlinear equation[48, 49]:

$$A = X\mathrm{e}^{-kt} + E \tag{6}$$

where A, and k are the absorbance of M.R. in irradiation time of t, and the pseudo-first-order rate constant,. X and E are the amplitude and the endpoint of the photodegradation process. The photodegradation rate constant (k) for a period of 100 min in presence of the $Bi_{1\text{-}x}$ Sm_x FeO_3 were 0.00643, 0.0103, 0.0115, 0.0199, and 0.0118 Cm^{-1} for $x = 0.00$, 0.02, 0.04, 0.06, and 0.08 at pH 3.0. Besides, the K values of the $Bi_{0.094}$ $Sm_{0.06}$ $Fe_{1\text{-}y}$ Ni_yO_3 nanoparticles as a photocatalysts for a period of 60 min were 0.0173, 0.0287, 0.0604, 0.0324 Cm^{-1} for $y = 0.0$, 0.01, 0.03, and 0.05 (Table 5). The results showed that the M.R. degradation reaction rate increases significantly with the Sm and Ni dopants in the BFO lattice structure.

Conclusion

In this research, two BFO derivatives including, $Bi_{(1-x)}Sm_xFeO_3$ ($x = 0.1$, 0.08, 0.06, 0.04, 0.02) and $Bi_{0.094}$ $Sm_{0.06}$ Fe_{1-y} Ni_yO_3 nanoparticles ($y = 0.05$, 0.03, 0.01) were synthesized by sol–gel method and their application as photocatalyst for methyl red

Table 5 The kinetic study of M.R. photodegradation with the prepared nanoparticles

Nanoparticles	Time (min)	$K_1 \pm S$	$X \pm S$	$E \pm S$	R^2
$BiFeO_3$	100	0.00649 ± 0.004	1.853 ± 0.729	− 0.844 ± 0.749	0.985
$Bi_{0.98}Sm_{0.02}FeO_3$	100	0.0103 ± 0.003	1.325 ± 0.260	− 0.333 ± 0.276	0.986
$Bi_{0.96}Sm_{0.04}FeO_3$	100	0.0115 ± 0.004	1.279 ± 0.225	− 0.279 ± 0.241	0.985
$Bi_{0.94}Sm_{0.06}FeO_3$	100	0.0199 ± 0.003	1.020 ± 0.054	− 0.0211 ± 0.0583	0.993
$Bi_{0.92}Sm_{0.08}FeO_3$	100	0.0118 ± 0.003	1.271 ± 0.17	− 0.264 ± 0.183	0.990
$Bi_{0.94}Sm_{0.06}FeO_3$	60	0.0173 ± 0.004	1.288 ± 0.174	− 0.257 ± 0.187	0.990
$Bi_{0.94}Sm_{0.06}Fe_{0.99}Ni_{0.01}O_3$	60	0.0288 ± 0.002	1.047 ± 0.032	− 0.050 ± 0.035	0.997
$Bi_{0.94}Sm_{0.06}Fe_{0.97}Ni_{0.03}O_3$	60	0.0603 ± 0.002	0.895 ± 0.014	0.105 ± 0.010	0.998
$Bi_{0.94}Sm_{0.06}Fe_{0.95}Ni_{0.05}O_3$	60	0.0324 ± 0.005	0.968 ± 0.060	0.0045 ± 0.064	0.987

degradation were investigated. The study of the photocatalytic activities of Sm-doped BFO and Sm and Ni co-doped BFO for the M.R. degradation was performed under dark and visible light in hydrogen peroxide in an acidic media (pH 3.0). The photocatalytic activity of Sm and Ni co-doped BFO nanoparticles is higher than the Sm-doped BFO nanoparticles, showing the energy band-gap of the Sm and Ni co-doped BFO nanoparticles is lower than the Sm-doped BFO nanoparticles. Besides, the M.R. degradation time in the presence of $Bi_{0.94}Sm_{0.06}Ni_{0.03}Fe_{0.97}$ nanoparticles (about 60 min) is dramatically less than $Bi_{094}Sm_{0.06}FeO_3$ nanoparticles (about 100 min). The greater magnetic property of the Sm and Ni co-doped BFO nanoparticles compared to the Sm-doped BFO nanoparticles leads to a simple photocatalytic separation using a strong magnet after the M.R. degradation and removal of the centrifuge step. Under the optimum conditions, The MR degradation efficiencies under visible-light illumination for 60 and 105 min at pH 3.0 were 97.34 and 85.76% for $Bi_{0.94}Sm_{0.06}Ni_{0.03}Fe_{0.97}$ and $Bi_{094}Sm_{0.06}FeO_3$ nanoparticles.

Supplementary Information The online version contains supplementary material available at https://doi.org/10.1007/s11144-022-02281-z.

Acknowledgements The Azad University of Mashhad, Iran and Semnan University, Iran, are appreciated.

Author contributions All authors contributed to the study conception and design. AS, RSK, DSK and ZE: Material preparation, data collection and analysis were performed. AS: The first draft of the manuscript was written. and all authors commented on previous versions of the manuscript. All authors read and approved the final manuscript.

Funding The authors declare that no funds, grants, or other support were received during the preparation of this manuscript.

Data availability All data generated or analyzed during this study are included in this published article (and its supplementary information files).

Declarations

Conflict of interest The authors have no relevant financial or non-financial interests to disclose.

Ethical approval Disclosure of potential conflicts of interest

References

1. Ponraj C, Vinitha G, Daniel J (2017) A review on the visible light active $BiFeO_3$ nanostructures as suitable photocatalyst in the degradation of different textile dyes. Environ Nanotechnol Monit Manag. 7:110–120
2. Singh S, Sharma R, Khanuja M (2018) A review and recent developments on strategies to improve the photocatalytic elimination of organic dye pollutants by BiOX (X= Cl, Br, I, F) nanostructures. Korean J Chem Eng 35(10):1955–1968
3. Islam MA (2019) Emergent environmental pollutants removal using metal oxide nanoparticles. Cell 1818:482533

4. Mathew S, Radhakrishnan E (2019) Polymer nanocomposites alternative to reduce environmental impact of non-biodegradable food packaging materials. In: Ahmed S, Chaudhry SA (eds) Composites for Environmental Engineering. Wiley, New Jersey
5. Gordi Z, Ghorbani M, Ahmadian Khakhiyani M (2020) Adsorptive removal of enrofloxacin with magnetic functionalized graphene oxide@ Metal-organic frameworks employing D-optimal mixture design. Water Environ Res 92:1935–1947
6. Nowakowska M, Szczubiałka K (2017) Photoactive polymeric and hybrid systems for photocatalytic degradation of water pollutants. Polym Degrad Stab 145:120–141
7. He D, Luo Y, Lu S, Liu M, Song Y, Lei L (2018) Microplastics in soils: analytical methods, pollution characteristics and ecological risks. TrAC, Trends Anal Chem 109:163–172
8. Paliwal A, Banu R, Ameta R, Ameta SC (2017) Photocatalytic degradation of methylene blue using undoped and Co-doped bismuth ferrite. J Applicable Chem 6:967–975
9. Liu H, Wang C, Wang G (2020) Photocatalytic advanced oxidation processes for water treatment: recent advances and perspective. Chem Asian J 15:3239–3253
10. Lam S-M, Sin J-C, Mohamed AR (2017) A newly emerging visible light-responsive $BiFeO_3$ perovskite for photocatalytic applications: a mini review. Mater Res Bull 90:15–30
11. Bhoi YP, Mishra B (2018) Photocatalytic degradation of alachlor using type-II $CuS/BiFeO_3$ heterojunctions as novel photocatalyst under visible light irradiation. Chem Eng J 344:391–401
12. Irfan S, Shen Y, Rizwan S, Wang HC, Khan SB, Nan CW (2017) Band-gap engineering and enhanced photocatalytic activity of Sm and Mn doped $BiFeO_3$ nanoparticles. J Am Ceram Soc 100:31–40
13. Xie W, Li R, Xu Q (2018) Enhanced photocatalytic activity of Se-doped TiO_2 under visible light irradiation. Sci Rep 8:1–10
14. Gong Y, Zhao X, Zhang H, Yang B, Xiao K, Guo T, Zhang J, Shao H, Wang Y, Yu G (2018) MOF-derived nitrogen doped carbon modified g-C_3N_4 heterostructure composite with enhanced photocatalytic activity for bisphenol A degradation with peroxymonosulfate under visible light irradiation. Appl Catal B 233:35–45
15. Liang S, Zhang D, Yao X, Han R, Zhang Q, Jin C, Pu X, Geng Y (2020) Deposition-precipitation synthesis of Yb^{3+}/Er^{3+} co-doped BiOBr/AgBr heterojunction photocatalysts with enhanced photocatalytic activity under Vis/NIR light irradiation. Sep Purif Technol 238:116450
16. Yousefi R, Beheshtian J, Seyed-Talebi SM, Azimi H, Jamali-Sheini F (2018) Experimental and theoretical study of enhanced photocatalytic activity of Mg-doped ZnO NPs and ZnO/rGO nanocomposites. Chem Asian J 13:194–203
17. Bui TS, Bansal P, Lee B-K, Mahvelati-Shamsabadi T, Soltani T (2020) Facile fabrication of novel Ba-doped g-C_3N_4 photocatalyst with remarkably enhanced photocatalytic activity towards tetracycline elimination under visible-light irradiation. Appl Surf Sci 506:144184
18. Si Y-H, Xia Y, Shang S-K, Xiong X-B, Zeng X-R, Zhou J, Li Y-Y (2018) Enhanced visible light driven photocatalytic behavior of $BiFeO_3$/reduced graphene oxide composites. Nanomaterials 8:526
19. de Lima AF (2020) Optical properties, energy band gap and the charge carriers' effective masses of the R3c $BiFeO_3$ magnetoelectric compound. J Phys Chem Sol 144:109484
20. Verma MK, Kumar A, Das T, Kumar V, Singh S, Rai VS, Prajapati D, Sonwani RK, Sahoo K, Mandal K (2020) $BiFeO_3$ perovskite as an efficient photocatalyst synthesised by soft chemical route. Mater Technol 36:1–9
21. Naeimi A, Dehghan E, Khoshnoud DS, Gholizadeh A (2015) Enhancment of ferromagnetism in Ba and Er co-doped $BiFeO_3$ nanoparticles. J Magn Magn Mater 393:502–507
22. Rezaei M, Sanavi Khoshnoud D, Dehghan E (2016) Study of structural and magnetic properties of $BiFeO_3$ nanoparticles co-doped with Ba and La. Iranian J Crystallogr Miner 24:563–572
23. Yang Y, Kang L, Li H (2019) Enhancement of photocatalytic hydrogen production of $BiFeO_3$ by Gd^{3+} doping. Ceram Int 45:8017–8022
24. Zhang L, Feng W, Wang B, Wang K, Gao F, Zhao Y, Liu P (2017) Construction of dual-channel for optimizing Z-scheme photocatalytic system. Appl Catal B 212:80–88
25. Tang J, Wang R, Liu M, Zhang Z, Song Y, Xue S, Zhao Z, Dionysiou DD (2018) Construction of novel Z-scheme $Ag/FeTiO_3/Ag/BiFeO_3$ photocatalyst with enhanced visible-light-driven photocatalytic performance for degradation of norfloxacin. Chem Eng J 351:1056–1066
26. Rahimkhani M, Khoshnoud DS, Ehsani M (2018) Origin of enhanced multiferroic properties in $Bi_{0.85-x}La_{0.15}HoxFeO_3$ nanopowders. J Magn Magn Mater 449:538–544
27. Vanga PR, Mangalaraja R, Ashok M (2015) Effect of (Nd, Ni) co-doped on the multiferroic and photocatalytic properties of $BiFeO_3$. Mater Res Bull 72:299–305

28. Dehno RT, Khoshnoud DS (2022) Multiferroic properties in $Sm_{1-x}Er_xFeO_3$ ceramics. J Magn Magn Mater 541:168515
29. Irfan S, Li L, Saleemi AS, Nan C-W (2017) Enhanced photocatalytic activity of La^{3+} and Se^{4+} co-doped bismuth ferrite nanostructures. J Mater Chem 5:11143–11151
30. Khoshnood RS, Khoshnoud DS (2019) Structural, magnetic, and photocatalytic properties in $Bi_{0.83-x}La_{0.17}Y_xFeO_3$ nanoparticles. Appl Phys A 125:1–10
31. Ghosh MP, Mukherjee S (2019) Disordered surface spins induced large exchange anisotropy in single-phase Sm^{3+} ions substituted nickel ferrite nanoparticles. J Magn Magn Mater 489:165320
32. Yang YL, Yang XC, Yuan JY, Li T, Fan YT, Wang L, Deng Z, Li QL, Wan DY, Zhao JT (2021) Time-Resolved Bright Red to Cyan Color Tunable Mechanoluminescence from CaZnOS: Bi3+, Mn2+ for Anti-Counterfeiting Device and Stress Sensor. Adv Opt Mater 9:2100668
33. Li Q, Bao S, Liu Y, Li Y, Jing Y, Li J (2016) Influence of lightly Sm-substitution on crystal structure, magnetic and dielectric properties of $BiFeO_3$ ceramics. J Alloy Compd 682:672–678
34. S. Ahammod Ali, (2018) Fabrication and characterization of $Ni_{1-x}Co_xFe_2O_4$ electromagnetic ceramic. http://lib.buet.ac.bd:8080/xmlui/handle/123456789/5732
35. Raevski I, Kubrin S, Pushkarev A, Olekhnovich N, Radyush Y, Li G, Chou C-C, Raevskaya S, Titov V, Malitskaya M (2019) Magnetic phase transitions in solid solutions of Fe-containing perovskite multiferroics. Ferroelectrics 542:36–44
36. Puhan A, Bhushan B, Satpathy S, Meena S, Nayak A, Rout D (2019) Facile single phase synthesis of Sr, Co co-doped $BiFeO_3$ nanoparticles for boosting photocatalytic and magnetic properties. Appl Surf Sci 493:593–604
37. Nadeem M, Khan W, Khan S, Shoeb M, Husain S, Mobin M (2018) Significant enhancement in photocatalytic performance of Ni doped $BiFeO_3$ nanoparticles. Mater Res Expr 5:065506
38. Zedek R, Djedjiga H, Megherbi M, Belkaid MS, Ntsoenzok E (2021) Effects of slight Fe (III)-doping on structural and optical properties of TiO_2 nanoparticles. J Sol-Gel Sci Technol 100:44–54
39. Haruna A, Abdulkadir I, Idris S (2020) Photocatalytic activity and doping effects of $BiFeO_3$nanoparticles in model organic dyes. Heliyon 6:e03237
40. Thammanu S, Marod D, Han H, Bhusal N, Asanok L, Ketdee P, Gaewsingha N, Lee S, Chung J (2021) The influence of environmental factors on species composition and distribution in a community forest in Northern Thailand. J For Res 32:649–662
41. Liao C, Tian Q, Liu F (2021) Nitrogen availability regulates deep soil priming effect by changing microbial metabolic efficiency in a subtropical forest. J For Res 32:713–723
42. Ghorbani M, Ariavand S, Aghamohammadhasan M, Seyedin O (2021) Synthesis and optimization of a green and efficient sorbent for removal of three heavy metal ions from wastewater samples: kinetic, thermodynamic, and isotherm studies. J Iran Chem Soc 18:1947–1963
43. Mohammadi P, Ghorbani M, Keshavarzi M, Rastegar A, Pakseresht M, Mohammadi M (2022) Dispersive micro solid-phase extraction as a green procedure for extracting prostate anti-cancer drugs in real water and biological samples and optimization of sorbent composite with an optimal mixture design. Int J Environ Anal Chem. https://doi.org/10.1080/03067319.2022.2045588
44. Rahmati R, Nayebi B, Ayati B (2021) Investigating the effect of hydrogen peroxide as an electron acceptor in increasing the capability of slurry photocatalytic process in dye removal. Water Sci Technol 83:2414–2423
45. Neshin MV, Khoshnood RS, Khoshnoud DS (2021) Enhanced photocatalytic activity of Ni-doped $BiFeO_3$ nanoparticles for degradation of bromophenol blue in aqueous solutions. React Kinet Mech Catal 134:951–970
46. Choi W, Termin A, Hoffmann MR (2002) The role of metal ion dopants in quantum-sized TiO_2: correlation between photoreactivity and charge carrier recombination dynamics. J Phys Chem 98:13669–13679
47. Hu Z, Chen D, Wang S, Zhang N, Qin L, Huang Y (2017) Facile synthesis of Sm-doped $BiFeO_3$ nanoparticles for enhanced visible light photocatalytic performance. Mater Sci Eng, B 220:1–12
48. Lente G (2015) Deterministic kinetics in chemistry and systems biology: the dynamics of complex reaction networks. Springer, Cham
49. Lente G (2018) Facts and alternative facts in chemical kinetics: remarks about the kinetic use of activities, termolecular processes, and linearization techniques. Curr Opin Chem Eng 21:76–83

Authors and Affiliations

Ava Saghafi[1] · Razieh Sanavi Khoshnood[1] · Davoud Sanavi Khoshnoud[1,2] · Zarrin Es'Haghi[1,3]

[1] Department of Chemistry, Mashhad Branch, Islamic Azad University, Mashhad, Iran

[2] Faculty of Physics, Semnan University, P. O. Box 35195-363, Semnan, Iran

[3] Department of Chemistry, Payam Noor University, Tehran, Iran